

Modeling of Interaction of Ions

with Ether- and Ester-linked phospholipids

by

Matthew W. Saunders

A thesis submitted in partial fulfillment  
of the requirements of the degree of  
Master of Science in Biology

with a concentration in Cell & Molecular Biology  
Department of Cell Biology, Microbiology and Molecular Biology  
College of Arts and Sciences  
University of South Florida

Major Professor: Sameer Varma, Ph.D.

Sagar Pandit, Ph.D.

H. Lee Woodcock, Ph.D.

Jianjun Pan, Ph.D.

# Contents

<b>List of Tables</b>	<b>ii</b>
<b>List of Figures</b>	<b>iii</b>
<b>Abstract</b>	<b>iv</b>
<b>1 Introduction</b>	<b>1</b>
1.1 Ether- and Ester-linked Phospholipids . . . . .	1
1.2 Using Molecular Dynamics to Study Biological Membranes? . . . . .	3
<b>2 Interaction of salt with ether- and ester-linked phospholipid bilayers</b>	<b>5</b>
2.1 Methods . . . . .	5
2.1.1 HOPC bilayer construction . . . . .	6
2.1.2 Simulation Details . . . . .	6
2.2 Results and Discussion . . . . .	7
2.2.1 Bilayer Structure . . . . .	7
2.2.2 Membrane-salt interactions . . . . .	10
2.2.3 Water structure and dynamics . . . . .	11
2.2.4 Bilayer electrostatics . . . . .	15
2.2.5 Salt distribution at the bilayer-solvent interface . . . . .	16
<b>3 Conclusions</b>	<b>30</b>
<b>Bibliography</b>	<b>31</b>
3.1 Supplemental Figures and Captions . . . . .	36

# List of Tables

2.1	Comparison of HOPC and POPC bilayer structure properties: $V_l$ is the lipid volume; $V_c$ and $V_h$ are
2.2	Diffusion coefficients of water measured in nm <sup>2</sup> /s in different regions along the bilayer normal (see Fig. 2)
2.3	Parameters in Gouy-Chapman theory. $K$ was calculated using equation 2.13. This was done using
S1	..... 37

# List of Figures

1.1	Representative image of a bilayer of phospholipids. The lipids can be seen in the center of the image.
1.2	Chemical structures of representative phospholipids highlighting the difference between ether- and ester-linked fatty acids.
2.1	Comparison of component mass densities between the HOPC and POPC systems. Densities are calculated for each lipid tail and headgroup.
2.2	Electron Densities of Simulated Systems. Symmetrized electron density distribution of each simulated system.
2.3	Order parameters of lipid chains. $S_{n_1}$ and $S_{n_2}$ refer to the two lipid tails. The carbon numbering scheme is shown for each tail.
2.4	Comparison of headgroup component and ion number densities between the HOPC and POPC systems.
2.5	First shell coordination environment of $\text{Na}^+$ ions. The cutoff distance for the first shell is taken as 6 Å.
2.6	Cumulative radial distribution functions of water hydrogens around various lipid oxygens. The distributions are shown for the headgroup oxygen and the carbonyl oxygens.
2.7	The first and second order parameters, $P_1$ and $P_2$ , of water O-H bonds. Each parameter is calculated for the first and second coordination shells.
2.8	Orientational autocorrelation times of O-H bonds in water, as determined by modeling their autocorrelation functions.
2.9	Comparison of electrostatic potentials between the HOPC and POPC systems. These distributions are shown for the headgroup oxygen and the carbonyl oxygens.
2.10	Illustration of bulk ion distribution, with surfaces used in Gouy-Chapman theory calculations. Four concentric spheres represent the first four coordination shells.
2.11	Comparison of Gouy-Chapman theory predictions and simulation results. Theoretical distributions are compared with simulation results for the first four coordination shells.
S1	38

# Abstract

Lorem ipsum dolor sit amet, consectetuer adipiscing elit. Ut purus elit, vestibulum ut, placerat ac, adipiscing vitae, felis. Curabitur dictum gravida mauris. Nam arcu libero, nonummy eget, consectetuer id, vulputate a, magna. Donec vehicula augue eu neque. Pellentesque habitant morbi tristique senectus et netus et malesuada fames ac turpis egestas. Mauris ut leo. Cras viverra metus rhoncus sem. Nulla et lectus vestibulum urna fringilla ultrices. Phasellus eu tellus sit amet tortor gravida placerat. Integer sapien est, iaculis in, pretium quis, viverra ac, nunc. Praesent eget sem vel leo ultrices bibendum. Aenean faucibus. Morbi dolor nulla, malesuada eu, pulvinar at, mollis ac, nulla. Curabitur auctor semper nulla. Donec varius orci eget risus. Duis nibh mi, congue eu, accumsan eleifend, sagittis quis, diam. Duis eget orci sit amet orci dignissim rutrum.

Nam dui ligula, fringilla a, euismod sodales, sollicitudin vel, wisi. Morbi auctor lorem non justo. Nam lacus libero, pretium at, lobortis vitae, ultricies et, tellus. Donec aliquet, tortor sed accumsan bibendum, erat ligula aliquet magna, vitae ornare odio metus a mi. Morbi ac orci et nisl hendrerit mollis. Suspendisse ut massa. Cras nec ante. Pellentesque a nulla. Cum sociis natoque penatibus et magnis dis parturient montes, nascetur ridiculus mus. Aliquam tincidunt urna. Nulla ullamcorper vestibulum turpis. Pellentesque cursus luctus mauris.

# Chapter 1

## Introduction

### 1.1 Ether- and Ester-linked Phospholipids

Phospholipids are a varied species of biological molecules used in many roles in life. These molecules are amphipathic, with a headgroup that is hydrophilic attached to hydrophobic acyl chains by a glycerol backbone [1]. These molecules can self assemble into many various structures in aqueous solution to reduce the exposure of the hydrophobic chains to polar solvent. Phospholipids tend to form bilayers, where the hydrophilic headgroups face the solvent and the hydrophobic lipid chains face into the center of the structure. These make up the primary structure of cell membranes found in most living things. An image of a bilayer of a model lipid can be seen in figure 1.1. Phospholipids have an incredible number of degrees of freedom in their chemical construction, and the structure of the individual molecules directly influences the stucture of assemblies of the lipids. Polar headgroups come in many varieties, and can be charged or zwitterionic. The fatty acid chains can be saturated or unsaturated, and can have many different lengths depending on the needs of the cell.

Phospholipids can also use several different types of chemical links between the glycerol backbone and the fatty acid chains. Phospholipids containing ether-links represent one of the many major evolutionary divides – while they make up much of the phospholipids of

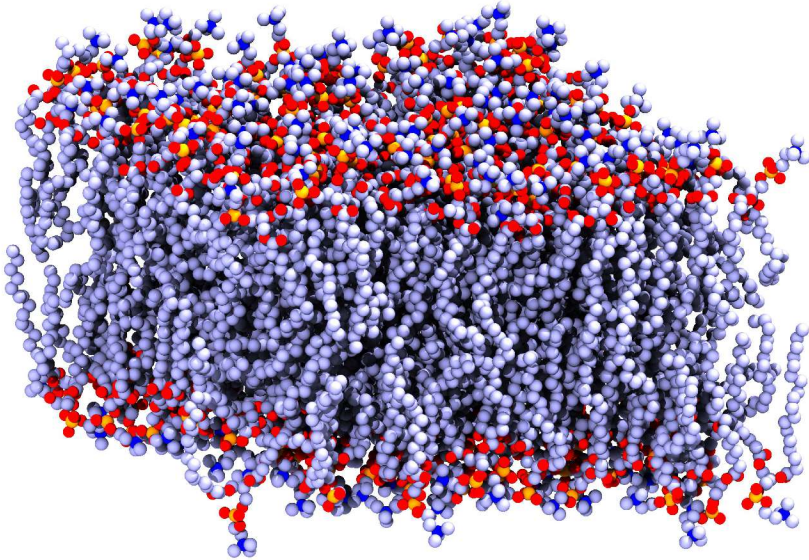


Figure 1.1: Representative image of a bilayer of phospholipids. The lipids can be seen in the center of the image, with the hydrophobic chains colored in light purple. The polar headgroup can be seen highlighted by the phosphate group in orange and the choline nitrogen in blue facing the solvent. The image also includes dissolved ions, which commonly interact with lipid bilayers. Solvent is not shown for clarity.

archaeal membranes, they are present in only small fractions in eukarya and bacteria [2, 3]. These phospholipids differ from the more common ester-linked phospholipids of bacterial and eukaryotic membranes in that they lack fatty acid carbonyl groups (see figure 1.2).

The chemical difference between ester- and ether-linked lipids has been shown to manifest into noticeable differences in bilayer properties, including both structure and permeability [4, 5, 6, 7, 8, 9]. Experiments show that model bilayers composed exclusively of ether-linked lipids have smaller dipole potentials compared to bilayers composed of their ester-linked analogs [6]; a result also predicted by a molecular dynamics (MD) study done by our group [9]. The interfacial water in ether-linked lipid bilayers is also more structured compared to that in ester-linked lipid bilayers, as observed in NMR experiments in the form a larger quadrupolar splitting constants [6], and as also reproduced in our simulations [9]. Two independent experimental studies also show that ether-linked lipid bilayers are less permeable to water compared to bilayers composed of their ester-linked analogs [5, 4].

Nevertheless, all studies aimed at examining differences between ester- and ether-linked

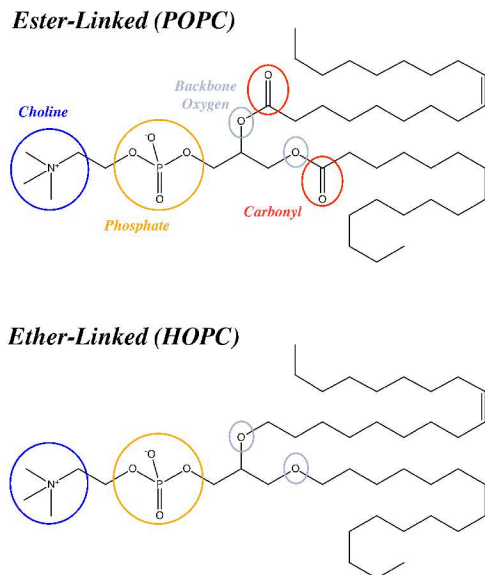


Figure 1.2: Chemical structures of representative phospholipids highlighting the difference between ether- and ester-links. POPC (1-palmitoyl-2-oleoyl-sn-glycero-3-phosphatidylcholine) is a diester lipid and HOPC (1-hexadecyl-2-(9-octadecenyl)-sn-glycero-3-phosphatidylcholine) is its diether analog that lacks fatty acid carbonyl groups.

lipid bilayers have been carried out in pure water, except for the one recent study by Leonard *et al.* [10]. As such, several studies show that salt significantly affects the properties of ester-linked lipid bilayers [11, 12, 13, 14, 15]. For example, in our previous work on the interactions of monovalent ions on zwitterionic ester-linked lipid bilayers [11] we found that monovalent cations insert into headgroup region. We reported reduction in area per lipid, increase in bilayer thickness, increased range of ordered solvent at the bilayer surface, and an increase in the electrostatic dipole potential of the bilayer.

## 1.2 Using Molecular Dynamics to Study Biological Membranes?

Computational modeling is a method commonly employed in order to study the atomistic details of the interactions that lead to the overall structure of lipid bilayers. Experiments utilizing methods such as NMR and x-ray scattering [6, 8, 16] are often used to inform and

develop computational models, which can then be used to predict how the overall structure occurs.

# Chapter 2

## Interaction of salt with ether- and ester-linked phospholipid bilayers

The general questions of how salt interacts with ether-linked lipid bilayers, and how ether-linked lipid bilayers differ from ester-linked lipid bilayers in the presence of salt is the objective of the current work. In our work, we addressed these questions by carrying out a molecular dynamics simulation of 1-hexadecyl-2-(9-octadecenyl)-sn-glycero-3-phosphatidylcholine lipid bilayer (HOPC) in NaCl salt. We also compared results of this simulation against our previous simulation of 1-palmitoyl-2-oleoyl-sn-glycero-3-phosphatidylcholine lipid bilayer (POPC) in NaCl [11]. Additionally, to gain insight into how salt modulates differences between ether- and ester-linked lipid bilayers, we also compared these simulations against those of ether- and ester-linked lipid bilayers in pure water [9].

### 2.1 Methods

The trajectories for the POPC bilayer in 200 mM NaCl were taken from our previous work [11], and were re-analyzed to address the specific goals of this project. The trajectories for the HOPC bilayer were generated as described below, following the same protocol we used for the POPC bilayer. Analysis was carried out using GROMACS [17, 18, 19, 20, 21]

utility tools, and in-house software developed using GROMACS API.

### 2.1.1 HOPC bilayer construction

To construct the HOPC bilayer, we first place 100 lipids on  $10 \times 10$  nm grid to form a bilayer leaflet, and then reflect the leaflet to create the second leaflet of the bilayer. We then introduce 30,000 water molecules into the space outside the bilayer, which gives a 150:1 waters to lipid ratio. We then replace 216 randomly-selected waters with 108  $\text{Na}^+$  and 108  $\text{Cl}^-$  ions to set an initial NaCl concentration of 200 mM. Note that the high water to lipid ratio is necessary to get a good representation of bulk solvent, as the addition of salt increases the distance of solvent ordering from the bilayer surface [11]. We then remove bad contacts by energy minimizing using the steepest descent approach. Finally, we subject the system to one cycle of annealing. Heating is done under constant pressure to 500K, but in steps of 100K to avoid excess kinetic energy divergence. During heating, each step is simulated for 10 ps. Cooling is also performed under constant pressure, but in smaller decrements – cooling from 500K to 400K is done in 5 steps, and cooling from 400K to 300K in steps of 10 steps. Each cooling step is simulated for 50 ps. The total annealing time is 850 ps.

### 2.1.2 Simulation Details

MD simulation is performed using GROMACS version 5.1.5 [17, 18, 19, 20, 21]. Water is described using the SPC/E model [22], and we use the united atom Gromos 43A1-S3 parameters for lipids and lipid-water cross terms developed by our group [23, 9]. These parameters have been verified in previous works without salt against experimental SAXS data to ensure accurate reproduction of bilayer structure [9]. Parameters for HOPC are derived from those for ether-linkages used for di-hexadecyl phosphatidylcholine developed for previous work without ions [9]. Ion-ion and ion-water interactions are described using parameters developed by Joung and Cheatham III [24], and the ion-lipid cross terms are calculated explicitly using Lorentz–Berthelot rules [11]. These ion parameters were verified

in previous work for binding constants as well as electrostatic potential, and we reported good reproduction of experimental results [11]. Temperature is held constant at 300K using the Nos  -Hoover thermostat [25], and a coupling constant of 0.5 ps. Pressure is maintained at 1 bar using the Parrinello-Rahman semisotropic barostat [26], and a pressure coupling constant of 1.5 ps. All bonds are constrained using the P-LINCS algorithm [27]. Neighbor-list is updated every other time step, and integration is carried out using the Verlet scheme. Long-range electrostatics beyond 16    are computed using the smooth particle mesh Ewald algorithm [28], and Lennard-Jones interactions are calculated with a cutoff of 16   . As before [11], a continuous MD simulation is run for 0.5   s.

## 2.2 Results and Discussion

### 2.2.1 Bilayer Structure

We first compare mass densities of the different chemical components of HOPC against those of POPC (see figure 2.1).

We find that the headgroup region of HOPC has a higher density of solvent compared to POPC – this is visible as a distinct peak in the solvent density profile in the HOPC system. We verified that this additional peak does not result from accumulation of ions, which we check by comparing mass density profiles of only water molecules. In fact, we had observed a similar, albeit smaller, water density peak in our previous simulation of another diether lipid bilayer in the absence of salt [9].

Table 2.1 compares the structural properties of HOPC and POPC bilayers. Lipid volumes  $V_l = V_c + V_{hg}$ , where  $V_c$  and  $V_{hg}$  are

the volumes of lipid chains (tails) and headgroups. These are computed using the approach given in Petrache et al. [29]. In this approach, we first compute the number densities  $n_i(z)$  of the various system components as a function of the bilayer normal ( $z$ ). We then use these  $n_i(z)$  to determine their partial molecular volumes,  $v_i$ , by optimizing the objective

	POPC with NaCl	HOPC with NaCl
$V_c$ ( $\text{\AA}^3$ )	$898.4 \pm 1.2$	$900.0 \pm 1.0$
$V_h$ ( $\text{\AA}^3$ )	$318.9 \pm 0.9$	$290.2 \pm 0.9$
$V_l$ ( $\text{\AA}^3$ )	$1217.3 \pm 0.5$	$1190.2 \pm 0.9$
$2D_c$ ( $\text{\AA}$ )	$30.95 \pm 0.32$	$32.13 \pm 0.25$
$D_b$ ( $\text{\AA}$ )	$46.22 \pm 0.49$	$46.05 \pm 0.34$
$A_l$ ( $\text{\AA}^2$ )	$58.07 \pm 0.63$	$56.03 \pm 0.45$
$D_{hh}$ ( $\text{\AA}$ )	$40.24 \pm 0.75$	$42.62 \pm 0.88$
$N_w$	22.6	22.3
$\Delta\nu$ (Hz)	194.99	1756.08

Table 2.1: Comparison of HOPC and POPC bilayer structure properties:  $V_l$  is the lipid volume;  $V_c$  and  $V_h$  are the partial volumes of lipids chains and headgroups, respectively;  $2D_c$  and  $D_b$  are chain and bilayer thickness, respectively;  $A_l = V_c/D_c$  is the area per lipid.  $N_w$  is the number of perturbed waters in the system, defined as those behind the *hydration boundary*.  $\Delta\nu$  is the quadrupolar splitting constant of each system.

function,

$$\Omega(v_i) = \sum_{z_j}^{n_s} \left(1 - \sum_{i=1}^{N_{\text{groups}}} (n_i(z_j)v_i)\right)^2. \quad (2.1)$$

Here,  $N_{\text{groups}} = 7$  are the different system components including methyls ( $v_{CH_3}$ ), methines ( $v_{CH_2}$ ), methylenes ( $v_{CH}$ ), headgroup carbons, headgroup and backbone oxygens, headgroup phosphate and nitrogen, and water ( $v_{H_2O}$ ). These partial volumes are shown in supplemental figure S1. Using these partial molecular volumes, we compute  $V_c = 2v_{CH_3} + 2v_{CH_1} + 28v_{CH_2}$  and  $V_{hg} = 10v_{hg_C} + 2v_{P\&N} + 8v_{hg_O}$ . We find that the headgroup volume of HOPC is  $27.1 \text{ \AA}^3$  smaller than POPC, due likely to the absence of carbonyl groups. As expected for lipids with the same hydrocarbon chains, the chain volumes are similar in the two lipids.

We also use the number densities computed above ( $n_i(z)$ ) to determine lipid chain thickness ( $2D_c$ ) and bilayer thickness ( $D_b$ ). This is done by first computing the probability of finding the  $i$ -th group in each slice of the simulation box,  $P_i(z) = n_i(z)/\sum_i n_i(z)$ . We define  $2D_c$  as the distance between the Gibbs' surfaces on the interfacial probability densities of lipid chains. Each of the two surfaces is computed by identifying the point on the curve where the integrals of probability densities in the interfacial regions above and below the surface are equal. We compute  $D_b$  in a similar manner, but from solvent probability densities. We find that both POPC and HOPC have similar membrane thicknesses ( $D_b$ ). Note, however, comparison of  $2D_c$  indicates that the hydrophobic chains in HOPC are slightly thicker than those in POPC, reflecting tighter chain packing. This is also evident from comparison of electron densities (see figure 2.2).

We often use the fourier-transform of the electron density to compare to experimental SAXS data; however, since such data is not available as far as we know, we cannot do this comparison. We have included this data in supplementary materials in case a comparsion becomes possible in the future (see supplemental figure S1). We also use the electron denisty distribution to calculate the peak-to-peak distance  $D_{hh}$ , another measure of the bilayer thickness. This discrepancy is likely due to the irregular shape of the distribution of solvent

in the headgroup of HOPC – the extra region of solvent accumulation may move the Gibbs' surface into the bilayer surface. This difference can be shown directly from comparison of chain order parameters (See figure 2.3).

We determine chain order parameters from the chain order tensor  $S_{\alpha\beta}$  defined as

$$S_{\alpha\beta} = \frac{1}{2} \left\langle 3 \cdot \cos(\theta_\alpha) \cdot \cos(\theta_\beta) - \delta_{\alpha\beta} \right\rangle, \quad (2.2)$$

where  $\theta_\alpha$  and  $\theta_\beta$  are the angles made by the molecular axes with  $\alpha$  and  $\beta$  as either  $x$ ,  $y$ , or  $z$ , and  $\delta_{\alpha\beta}$  is the Kronecker-delta function. For the saturated bonds [30]

$$-S_{CD}^{Sat} = \frac{2}{3}S_{xx} + \frac{1}{3}S_{yy}, \quad (2.3)$$

and for unsaturated bonds [16]

$$-S_{CD}^{Unsat} = \frac{1}{4}S_{zz} + \frac{3}{4}S_{yy} \mp \frac{\sqrt{3}}{2}S_{yz} \quad (2.4)$$

We then use  $V_c$  and  $D_c$  to calculate areas per lipid,  $A_l = V_c/D_c$ . We find that the lateral surface area of HOPC is slightly smaller than that of the POPC bilayer.

### 2.2.2 Membrane-salt interactions

Ions prefer to associate or coordinate with specific sites in the headgroup regions of the lipid bilayers (See figure 2.4) –  $\text{Na}^+$  ions near phosphates and  $\text{Cl}^-$  ions near cholines. Here we note that ion peaks are positioned similarly in both HOPC and POPC systems.  $\text{Cl}^-$  ions do not enter the bilayer headgroup region, while  $\text{Na}^+$  ions move far into this region of the bilayer surface. However, the  $\text{Na}^+$  densities trail off deeper into the POPC bilayer by  $\sim 5 \text{ \AA}$  (visible in the inset of figure 2.4). In fact, we find that more ions localize in the POPC bilayer – Averaged over the last 150 ns we see  $74.45 \pm 0.56$   $\text{Na}^+$  ions bound to POPC, compared to  $62.27 \pm 2.00$   $\text{Na}^+$  ions to HOPC. We consider an ion to be bound to the membrane when half

or fewer of the inner-shell coordination partners of the ion are waters. The inner shell of  $\text{Na}^+$  ions is defined using a cutoff of 3.15 Å based on radial distribution functions of  $\text{Na}^+$  with the water oxygens [31]. The  $\text{Cl}^-$  ions do not lose waters and do not seem to adsorb on the bilayer, hence we have not analyzed the binding behavior of  $\text{Cl}^-$  in this work. Figure 2.5 shows the inner-shell coordination environment of  $\text{Na}^+$  ions as a function of their positions in the bilayer. For this, we used a cutoff of 3.3 Å, based on the radial distribution functions of  $\text{Na}^+$  with the various lipid oxygens (data not shown). When  $\text{Na}^+$  ions are bound, they are primarily coordinated by phosphate oxygens – this holds for both HOPC and POPC. The main difference between POPC and HOPC is in how carbonyl oxygens, backbone oxygens and water oxygens coordinate with ions. In POPC, ions are also partially coordinated by carbonyl oxygens and water, but not by backbone oxygens. But in HOPC, backbone oxygens also partially coordinate  $\text{Na}^+$ . This may contribute to the deeper penetration of  $\text{Na}^+$  into the POPC bilayer, and the greater number of ions adsorbed onto the POPC bilayer surface when compared to HOPC.

### 2.2.3 Water structure and dynamics

As we noted above in Figure 2.1, the headgroup region of HOPC has a higher density of water than POPC. We have also noted previously that in general salts tend to extend the region of structured water near the bilayer surface [11]. To gain further insight into how the absence of carbonyl groups in ether lipid bilayers increases water density, we systematically characterize the structure and dynamics of water.

Figure 2.6 compares the integrated radial distribution of water hydrogens around lipid oxygens.

We note that there is very little water directly coordinating the backbone oxygens in the POPC bilayer ( $\sim 1/3$  water per lipid). Compared to backbone oxygens, more water directly coordinates the ester carbonyl oxygens and the phosphate oxygens in POPC. However, in HOPC we see a larger number of waters coordinating with the backbone oxygens, nearly 2

waters per lipid. Therefore, we attribute the higher density of water in HOPC to coordination with backbone oxygens.

Note that in POPC, carbonyls oxygens compete with phosphates for water coordination. Consequently, we expect waters to have a greater average ordering in the HOPC headgroup. In fact, this is what we had observed in our previous comparative study of diether- and diester-lipid bilayers [9].

In order to further explore solvent ordering by the bilayer surface, we compute order parameters of water O-H bonds. The first order parameter ( $P_1$ ) is calculated by time-averaging the cosine of the angle  $\theta$  that the OH bond makes with the bilayer normal, that is  $P_1 = \langle \cos(\theta) \rangle$ . Consequently, a positive value represents an orientation away the bilayer. The second parameter, which is defined as the second Legendre polynomial of  $\cos(\theta)$ , that is,  $P_2 = \langle (3 \cdot \cos^2(\theta) - 1) \rangle / 2$ . We calculate both  $P_1$  and  $P_2$  as a function of position along the bilayer normal, and they are shown in figure 2.7.

We find that the water in the headgroup region is clearly more ordered in the HOPC bilayer. Figure 2.7b shows the second order parameter. We note that the induced perturbations in the water layer are more prominent in HOPC than that of POPC. At the same time, however, we find that the numbers of water that are ordered in the two systems are similar. We count the average number of non-bulk (perturbed) waters as waters within the non-zero region of the second order parameter. We find this boundary by fitting an exponential function to the region starting at the peak in the first order parameter, and taking the inverse of the length-scale of the fitted function as the position of the surface. The region beyond this point is considered bulk water. We will refer to this surface as the *hydration boundary* for the remainder of the paper. For the purpose of counting the number of waters in the surface, we truncated the box at this boundary, to a length of 35 ångströms. Numbers of perturbed waters per lipid for each system can be seen in table 2.1 line 8.

We also use these order parameters to compute the quadrupolar splitting of water as measured in NMR. It is essentially a weighted average of the second order parameter, similar

to the one derived by Kruczak *et al.* [9]:

$$\Delta\nu = \frac{3}{4}\chi \frac{1}{N_w} \sum_{z_i=0}^{z_0} n_w(z_i) P_2(z_i), \quad (2.5)$$

where the number of perturbed waters in the system is  $N_w$ ,  $n_w$  is the number of waters in each slice of the box, and  $P_2(z_i)$  is the value of the second order parameter in the  $i^{\text{th}}$  slice. We take the quadrupolar splitting constant of water  $\chi = 220\text{KHz}$  from Åman *et al.* [32]. The summation over slices is carried out from the bilayer center ( $z = 0$ ) to the end of the box. We report that the quadrupolar splitting of water in the POPC system is 194.99 Hz, and that in the HOPC system is 1756.08 Hz (also shown in table 2.1, line 9). These values reflect a similar difference to what we observed in our earlier comparative study of ether- and ester-linked lipid bilayers in pure water [9].

Next we compute the lateral diffusion coefficient of water. To gain detailed insight, we compute it separately for four different regions along the bilayer normal. We define these regions using the  $P_2(z)$  profile:  $B_{-1}$  is the region closest to the bilayer center where  $P_2(z)$  is negative;  $B_+$  is the region where  $P_2(z)$  is positive;  $B_{-2}$  is the region beyond the  $B_+$  boundary where  $P_2(z)$  is negative; and the remaining portion beyond  $B_{-2}$  we refer to as bulk. These regions are also labeled in figure 2.7. The diffusion coefficients for waters in these regions are included in table 2.2. They are calculated using Einstein's relationship, and a

protocol detailed in our previous study [9]. Taking note of the overall pattern, the lateral diffusion decreases progressively as one moves deeper into the bilayer. Additionally, in the innermost regions –  $B_{-1}$  and  $B_+$  – water diffuses more slowly in HOPC compared to POPC. This result is similar to what we observed previously [9] in simulations without salt.

To characterize the orientational dynamics of waters, we compute autocorrelations of the their O-H bonds,

$$C^{O-H}(t) = \left\langle \vec{v}_{O-H}(0) \cdot \vec{v}_{O-H}(t) \right\rangle. \quad (2.6)$$

We calculate expectation values separately for all of the 2 Å slices along the bilayer normal by

	$B_{-1}$ ( $\text{nm}^2/\text{s}$ )	$B_+$ ( $\text{nm}^2/\text{s}$ )	$B_{-2}$ ( $\text{nm}^2/\text{s}$ )	Bulk ( $\text{nm}^2/\text{s}$ )
HOPC	$0.85 \pm 0.59$	$1.783 \pm 0.94$	$16.1 \pm 5.24$	$26.67 \pm 0.65$
POPC	$1.075 \pm 0.62$	$3.078 \pm 0.74$	$16.27 \pm 5.19$	$27.30 \pm 0.66$

Table 2.2: Diffusion coefficients of water measured in  $\text{nm}^2/\text{s}$  in different regions along the bilayer normal (see figure 2.7 and related text for the definitions of the different spatial regions. The two innermost-bilayer regions  $B_{-1}$  and  $B_+$  in HOPC contain waters that have a greatly lowered diffusion coefficient. In the regions  $B_{-2}$  and bulk, the bilayer composition does not seem to change the diffusion behavior. These values were calculated using the method outlined in previous work by our lab [9] The various regions are illustrated on figure 2.7.

tracking individual water molecules for 500ps, and also averaging over all waters in the slice. We also weight each water by the fraction of duration it spends in each slice. This is done in 5 ns chunks, and then averaged over the trajectories. We then model these autocorrelation as a sum of three exponential terms, that is,

$$C^{O-H}(t) = A_1 e^{-t/\tau_1} + A_2 e^{-t/\tau_2} + (1 - A_1 - A_2) e^{-t/\tau_3}, \quad (2.7)$$

where  $A_i$  are positive, and  $\tau_i$  are correlation times. Fitting is carried out using the Marquardt-Levenberg least-squares fitting method. The correlation times are plotted in figure 2.8.

We find that  $\tau_1$  shows a profile similar to what we observed for ether- and ester-lipids simulated in pure water [9]. Additionally, we find that the correlation times  $\tau_1$  and  $\tau_2$  in the HOPC bilayer are all longer than in POPC. The maximum correlation times of 1838 ps in HOPC and 1019 ps in POPC are characteristic of rotationally immobile waters inside the bilayer surface and also of crystallographically-resolved waters in protein-protein interfaces [33]. Note that  $\tau_3$ , which is of the order of picoseconds, is close to the sampling time of our trajectories. Thus we regard it simply as a fitting parameter.

Overall, we find that the headgroup water in HOPC is significantly more organized and also diffuses more slowly as compared to the headgroup water in POPC. This is similar to what we had observed [9] when we compared another diester lipid bilayer against its

chemically analogous diester-lipid bilayer, but in the absence of NaCl. This leads us to conclude that in ether-linked lipid bilayers water forms a rigid and immobile layer within the headgroup region of the bilayer, and exposure to a moderate concentration of salt does not disrupt this layer; this keeps the bilayer more rigid than the ester-linked analogue.

#### 2.2.4 Bilayer electrostatics

The dipole potential of a bilayer is the potential difference between the inside of the bilayer and bulk water. In our previous comparative study of ether- and ester-linked bilayers in pure water, [9] we had found that, consistent with experiment [6], the dipole potential of the ether-linked lipid bilayer was  $56 \pm 5$  mV smaller than that of the ester-linked lipid bilayer. We also know that membrane association with salt can modify its dipole potential, with increases of around 200mV from that of a bilayer without salt reported previously [11, 34, 35].

Figure 2.9 compares the electrostatic potential in HOPC and POPC as a function of distance along the bilayer normal.

These are calculated from an integration of the one dimensional Poisson's equation,

$$\phi(z) = -\frac{1}{\epsilon_0} \int_0^z \int_0^{z'} \rho(z) dz dz' + C_1 z + C_2, \quad (2.8)$$

where  $\rho(z)$  is the charge density along the bilayer normal, and  $\epsilon_0$  is the vacuum permittivity. Note that we integrate this equation using two boundary conditions – the electric field in bulk water is zero, which yields  $C_2 = 0$ , and the potential at the simulation box boundary is also zero, which makes  $C_1 = 0$ .

The first observation we make is that the dipole potentials of both HOPC and POPC are similar; a behavior distinct from that observed in simulations in pure water. Nevertheless, the overall electrostatic potential profiles are similar to those observed in pure water. Firstly, a characteristic peak near the phosphate region still exists, and this peak is higher for the diether lipid bilayer. This could potentially serve as a higher permeation barrier in the

diether-linked lipid system. This interpretation is consistent with our observation above that there are fewer membrane-associated ions in HOPC compared to POPC. Secondly, the diether-linked lipid system had a trough next to the peak, which is absent in the diester-linked lipid bilayer, and may serve as a trap for solvent molecules. In fact, the spatial location of the trough corresponds to the high water density region in the HOPC bilayer.

### 2.2.5 Salt distribution at the bilayer-solvent interface

The behavior of salt near bilayer surfaces is often modeled using the Gouy-Chapman theory; a mean-field approximation that has its roots in Poisson-Boltzman theory [36, 37]. This theory also forms the basis for electrophoretic mobility studies [37]. In this theory, water is modeled as a dielectric continuum in which ion particles behave as an uncorrelated gas. So far, due to limitations from system size and ionic force field parameters, we have refrained from comparing or validating our simulations at the atomistic level against this theory. Here, we show convergence between these atomistic simulations and the Poisson-Boltzman theory.

Within the Poisson-Boltzmann theory, the number density of ions near the bilayer surface is described as

$$\rho(z) = \rho_0 \exp(-\bar{z}e\beta\psi(z)), \quad (2.9)$$

where  $\rho_0$  is the ion density in the bulk,  $\bar{z}$  is the valency of the ion,  $\beta = (k_b T)^{-1}$ ,  $e$  is the charge on an electron, and  $\psi(z)$  is the electrostatic potential. We define the interfaces as the *hydration boundaries* (see subsection 'Water structure and dynamics'). The lengths of the solvent occupied regions,  $D$ , in each of the two systems are listed in table 2.3. We set the center

of this solvent occupied region as  $z = 0$ , which them implies that the interfaces are essentially at  $z = \pm D/2$  nm , as illustrated in figure 2.10.

We model  $\psi(z)$  as a sum of two Debye-Huckle potentials [36], each a reflection of the

	$K(\text{nm}^{-1})$	$D \text{ nm}$	$\rho_0 (\text{nm}^{-3})$	$\sigma (e \text{ nm}^{-2})$
POPC	$0.98 \pm 0.021$	$13.167 \pm 0.0071$	$0.043 \pm 0.0018$	0.13
HOPC	$1.09 \pm 0.037$	$13.752 \pm 0.0068$	$0.060 \pm 0.0041$	0.128

Table 2.3: Parameters in Gouy-Chapman theory.  $K$  was calculated using equation 2.13. This was done using the value for  $\rho_0$  for each system, found by taking the average number density of  $\text{Cl}^-$  ions within the solvent-occupied region of the box. The charge density  $\sigma$  was calculated by integrating the charge of the ions from the bilayer center to the surface at 35 Å from the bilayer center for each system, shown to be the *hydration boundary* of both bilayers.  $D$  gives the length of the solvent-occupied region of each simulation box.

other around the center of the solvent occupied region:

$$\psi_1(z) = \psi_s \exp\left(-K(z + \frac{D}{2})\right) \quad (2.10)$$

$$\psi_2(z) = \psi_s \exp\left(K(z - \frac{D}{2})\right) \quad (2.11)$$

$$\psi(z) = \psi_1(z) + \psi_2(z) - (\psi_1(0) + \psi_2(0)) \quad (2.12)$$

Here  $\psi_s = \sigma/\epsilon_0\epsilon K$  is the electrostatic potential at the bilayer surface, where  $\sigma$  is the surface charge density of the bilayer leaflet [36].  $K$  is the inverse Debye length,

$$K = \sqrt{\sum_i \rho_{0,i} \bar{z}_i^2 \frac{e^2}{\epsilon_0 \epsilon k_b T}}, \quad (2.13)$$

where the sum of  $\rho_{0,i}$ 's is over all of the included ions in our system. Note that in Equ. 2.12 we subtract out the value of the potential at the center of the solvent occupied region from  $\psi(z)$ . Note also that the form of  $\psi_s$  is valid only for small surface potentials, generally those smaller than 20 millivolts [36]. Our systems have a relatively small surface charges (See table 2.3), which will result in small surface potentials (See table 2.3). The surface charges are calculated by integrating charge densities of ions contained behind the surface. We chose to do this because all other parts of the simulated system are uncharged, and the surface is entirely charged by the adsorbed ions.

Figure 2.11 compares the potential and ion distribution obtained from theory against those estimated directly from simulations.

We note a very close match between the two. Additionally, we find that HOPC shows a slightly larger  $K$  than POPC, indicating a  $\sim 10\%$  shorter screening length for the system. This means that a bilayer of HOPC is better shielded from environmental electric fields. The shorter screening length in the HOPC is also reflective of the smaller number of ions that adsorb onto the surface of the bilayer, as this directly results in a larger number density in bulk solvent due to the fixed number of ions in our system.

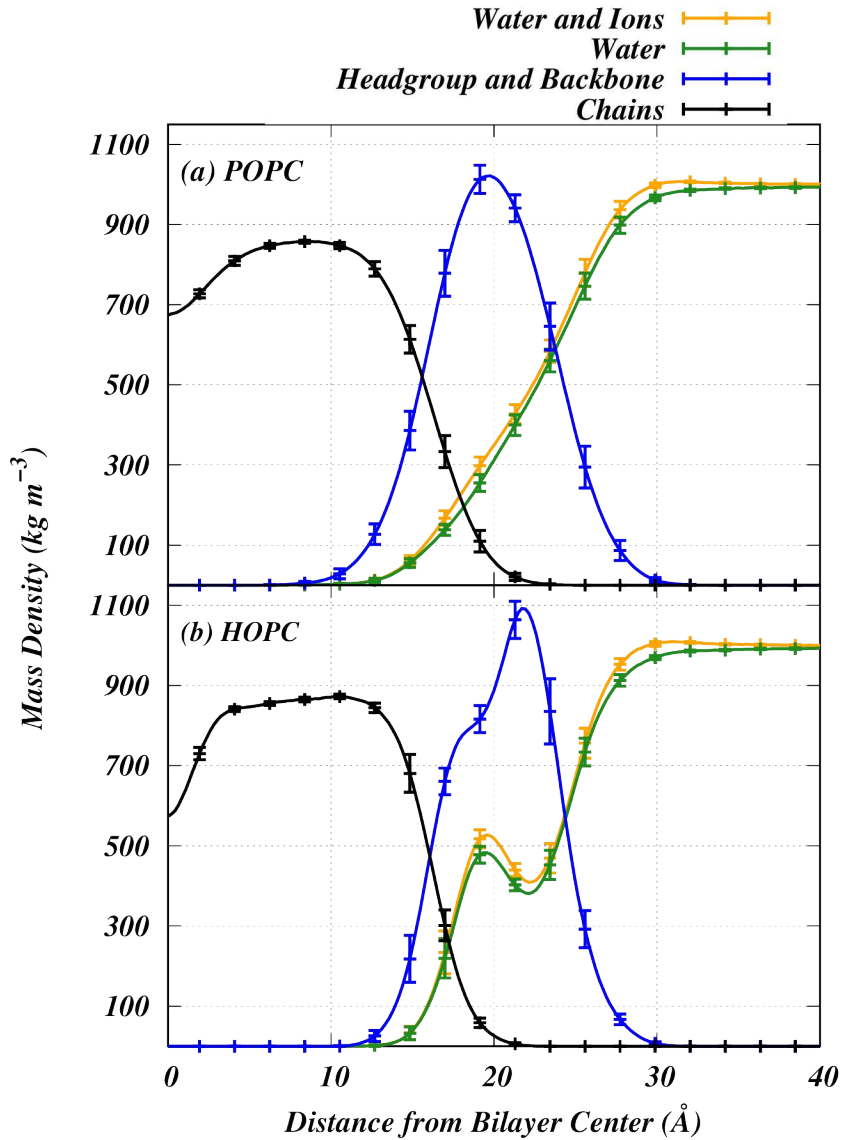


Figure 2.1: Comparison of component mass densities between the HOPC and POPC systems. Densities are computed by dividing the box dimension along the membrane normal into 2000 slices. For clarity of presentation, error bars are indicated for every 10th slice. Mass densities of solvent and ions, water, lipid headgroup and backbone, and lipid chains are shown. The plot for HOPC shows a peak in the water density inside the headgroup region that is not present in POPC, similar to what was seen in our previous work with DHPC [9].

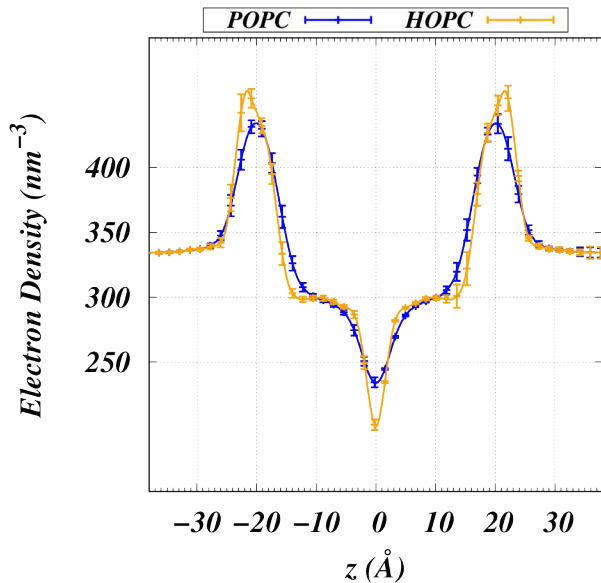


Figure 2.2: Electron Densities of Simulated Systems. Symmetrized electron density distribution of each simulated system as a function of  $z$ . We can see the distribution for HOPC is broader, with a longer peak-to-peak distance than in the POPC distribution. Furthermore, we see a deeper trough in the middle of the HOPC distribution. This plot was made by using the gromacs densities tool, dividing the system into 2000 slices. This data was calculated for every five nanoseconds, and averaged over the last 150ns of trajectories. Errorbars are shown for every 10th data point.

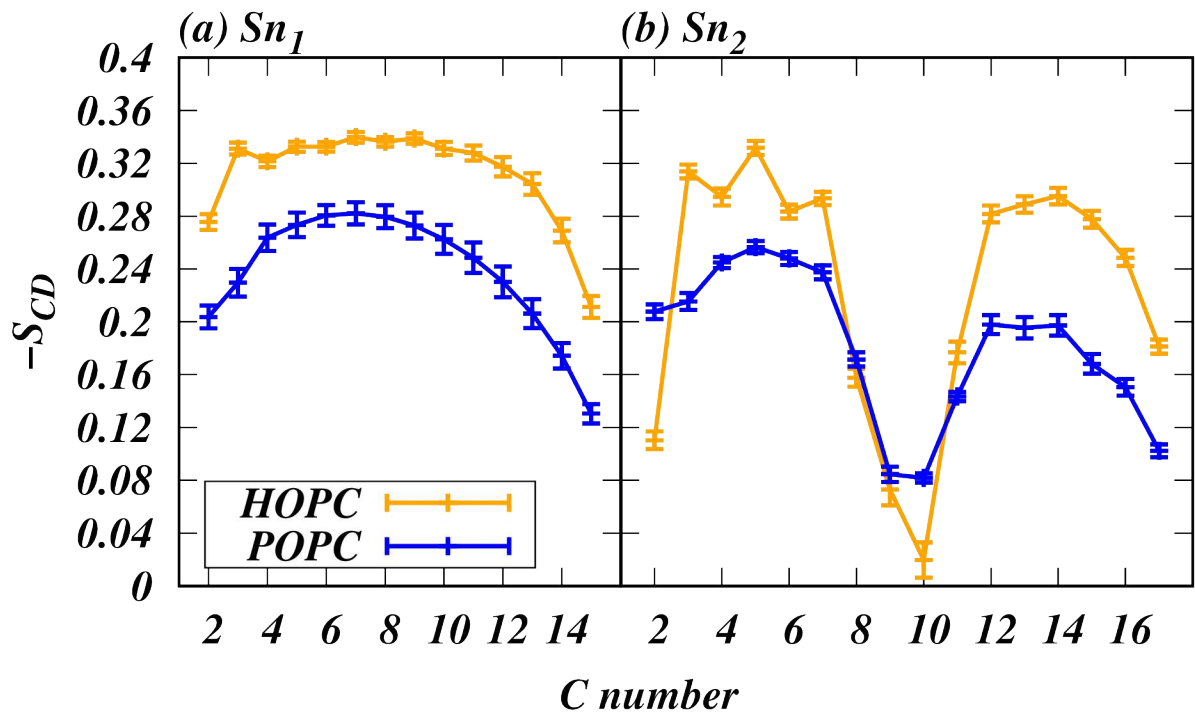


Figure 2.3: Order parameters of lipid chains.  $Sn_1$  and  $Sn_2$  refer to the two lipid tails. The carbon numbering starts from the polar carbon at the ester bond; however, we do not calculate an  $S_{CD}$  for the first carbon as this carbon would not have a hydrogen attached in an ester-linked lipid. This convention was maintained for the ether-linked lipid. The unsaturated bond is between carbons 9 and 10 on the  $Sn_2$  chain. In both chains, HOPC shows higher ordering, except for the unsaturated carbons on the 9-octadecene chain. This ordering corresponds with the lower area per lipid of the HOPC bilayer, values of which can be seen in table 2.1.

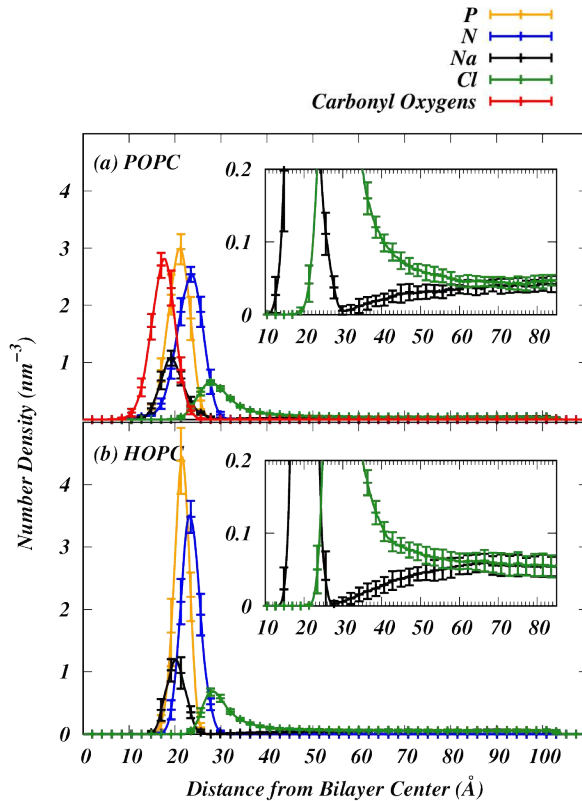


Figure 2.4: Comparison of headgroup component and ion number densities between the HOPC and POPC systems. The inset zooms in on the ordinate axis to added the extent of ion adsorption into bilayer as well as ion densities in the bulk. Densities are computed by dividing the box dimension along the membrane normal into 2000 slices. Error bars are indicated for every 10th slice. We note that sodium ions have a broader distribution in POPC than in HOPC. The peak of the  $\text{Na}^+$  distribution in POPC is also closer to the center of the bilayer than in HOPC. This may be due to the interaction of ions with the carbonyl oxygens (shown in red) that are present in POPC but absent in HOPC. In both bilayers, the chloride ions gather near the positively charged choline trimethylammonium, shown in blue. The inset shows the distribution of ions in the transitional region from the bilayer surface to bulk solvent. As one looks further out from the bilayer, the density of  $\text{Na}^+$  and  $\text{Cl}^-$  equalize, as is expected in bulk solvent.

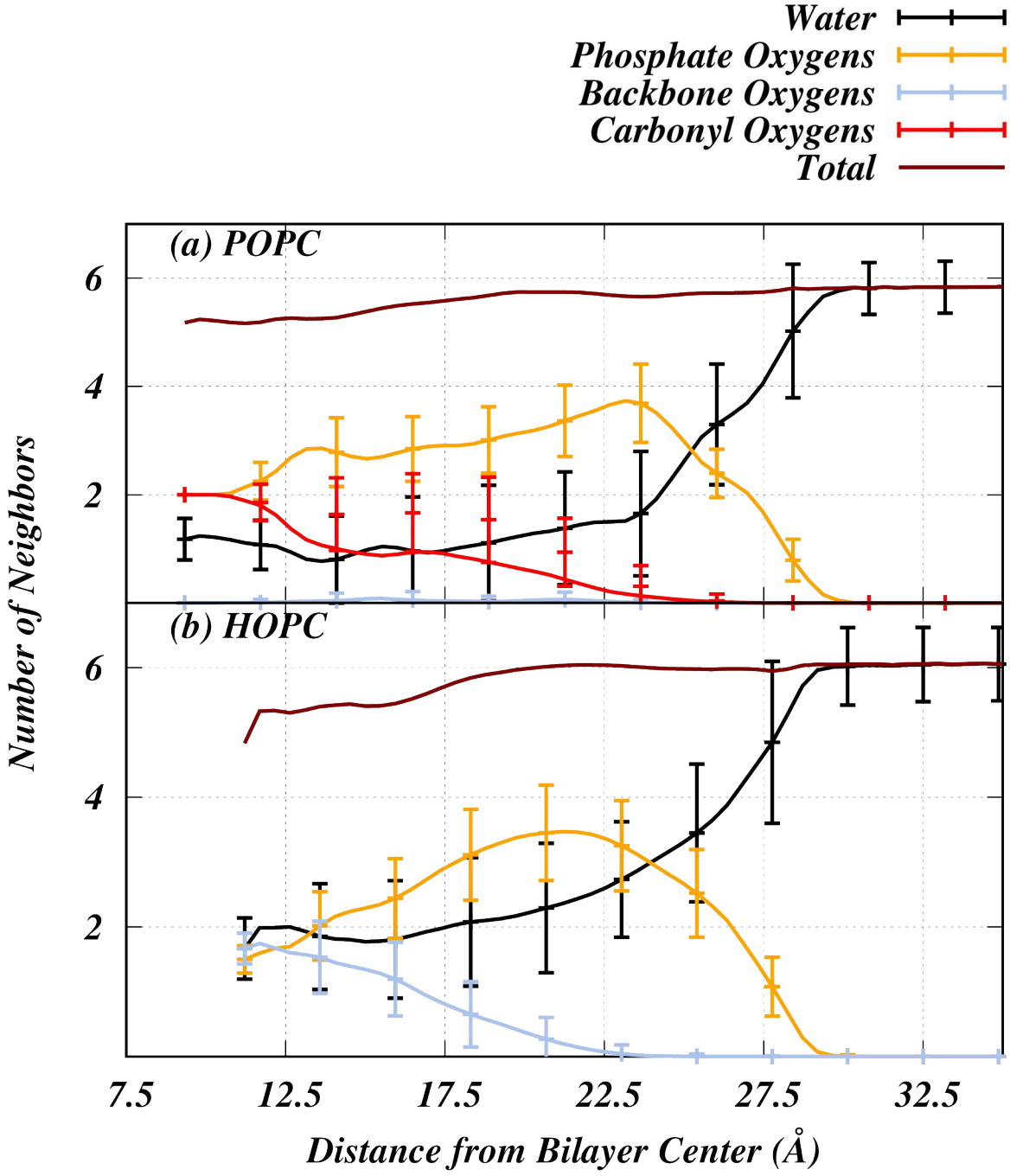


Figure 2.5: First shell coordination environment of  $\text{Na}^+$  ions. The cutoff distance for the first shell is taken as 3.3 ångströms, based on the radial distribution function of  $\text{Na}^+$  with the various lipid oxygens. This chart was made by dividing the box into 400 slices, and then symmetrizing around the bilayer center. Data is averaged over the last 100ns of simulation trajectory. Errorbars are shown for every tenth data point. Note that the coordination number of  $\text{Na}^+$  drops from 6 to 5 as it interacts deeper in both bilayers, and this drop occurs sooner in the HOPC system than in POPC. No values are shown for at distances less than 7.5 Å from the bilayer center, due to the lack of ions beyond in this region.

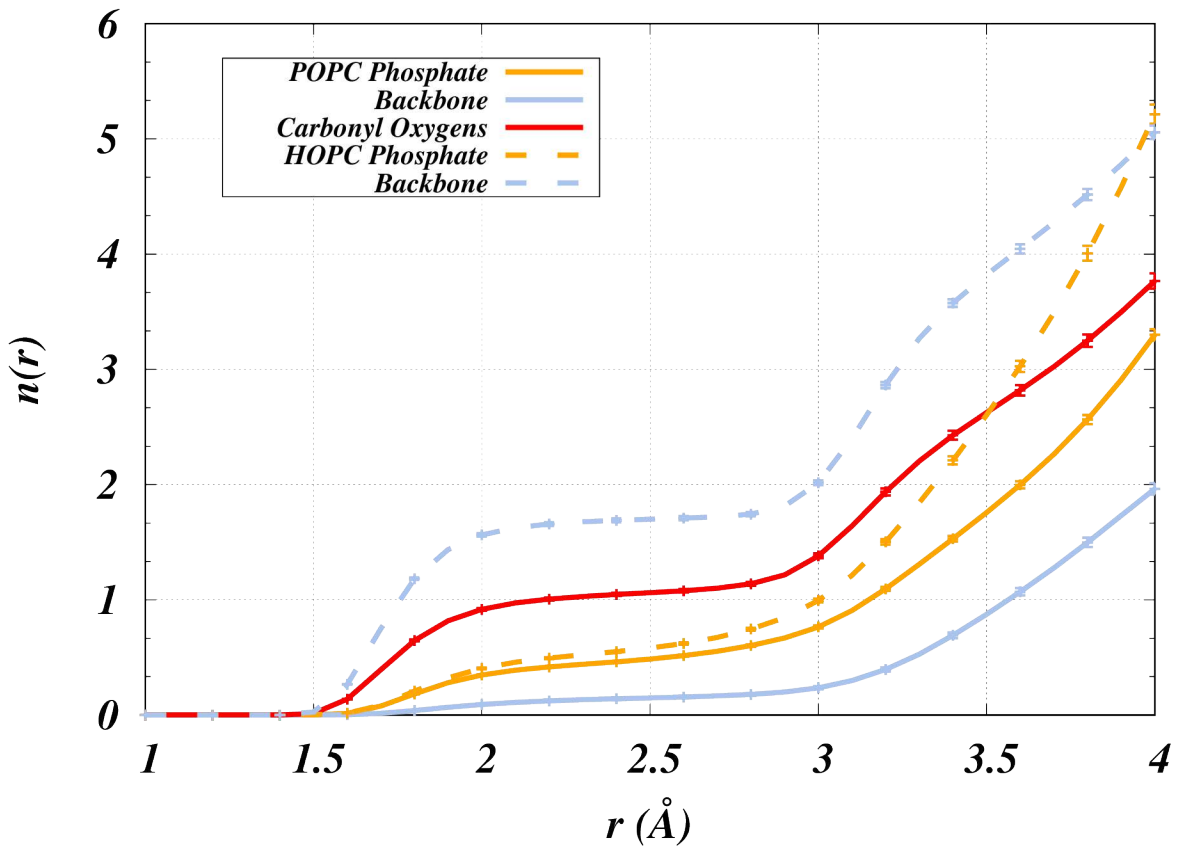


Figure 2.6: Cumulative radial distribution functions of water hydrogens around various lipid oxygens. The distributions for POPC are shown in solid lines, while HOPC is shown with dotted lines. The oxygens are grouped into categories as denoted in figure 1.2.

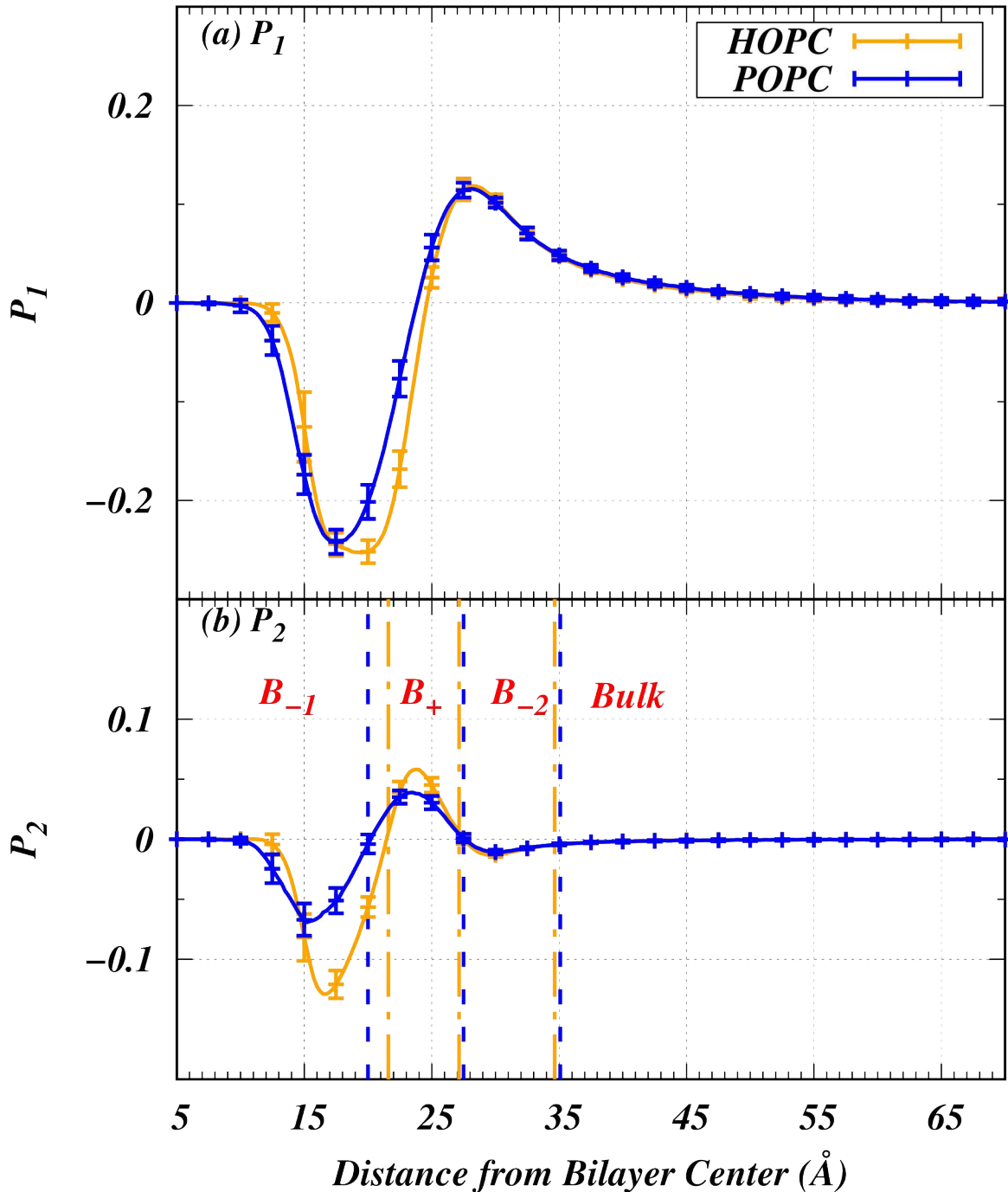


Figure 2.7: The first and second order parameters,  $P_1$  and  $P_2$ , of water O-H bonds. Each parameter is calculated by first dividing the simulation box into 2000 slices, and then averaging the data separately in each slice. The box is symmetrized around the bilayer center, and thus only half the box is shown. Standard deviations are calculated by dividing the trajectory into over 5ns blocks. The dashed vertical lines in the  $P_2$  plot are demarcations for the different spatial regions,  $B_{-1}$ ,  $B_+$ ,  $B_{-2}$ , and  $B_{\text{bulk}}$ , as discussed in the associated text.  $P_1$  is the average of the first legendre polynomial of the cosine of the angle between the bilayer normal and the O-H bond vector of each water molecule per box slice.  $P_2$  is the average of the second legendre polynomial. Looking to  $P_1$ , both systems exhibit similar magnitudes of ordering.  $P_2$  shows a more complicated distribution, with larger magnitudes of ordering in all regions in the HOPC system.

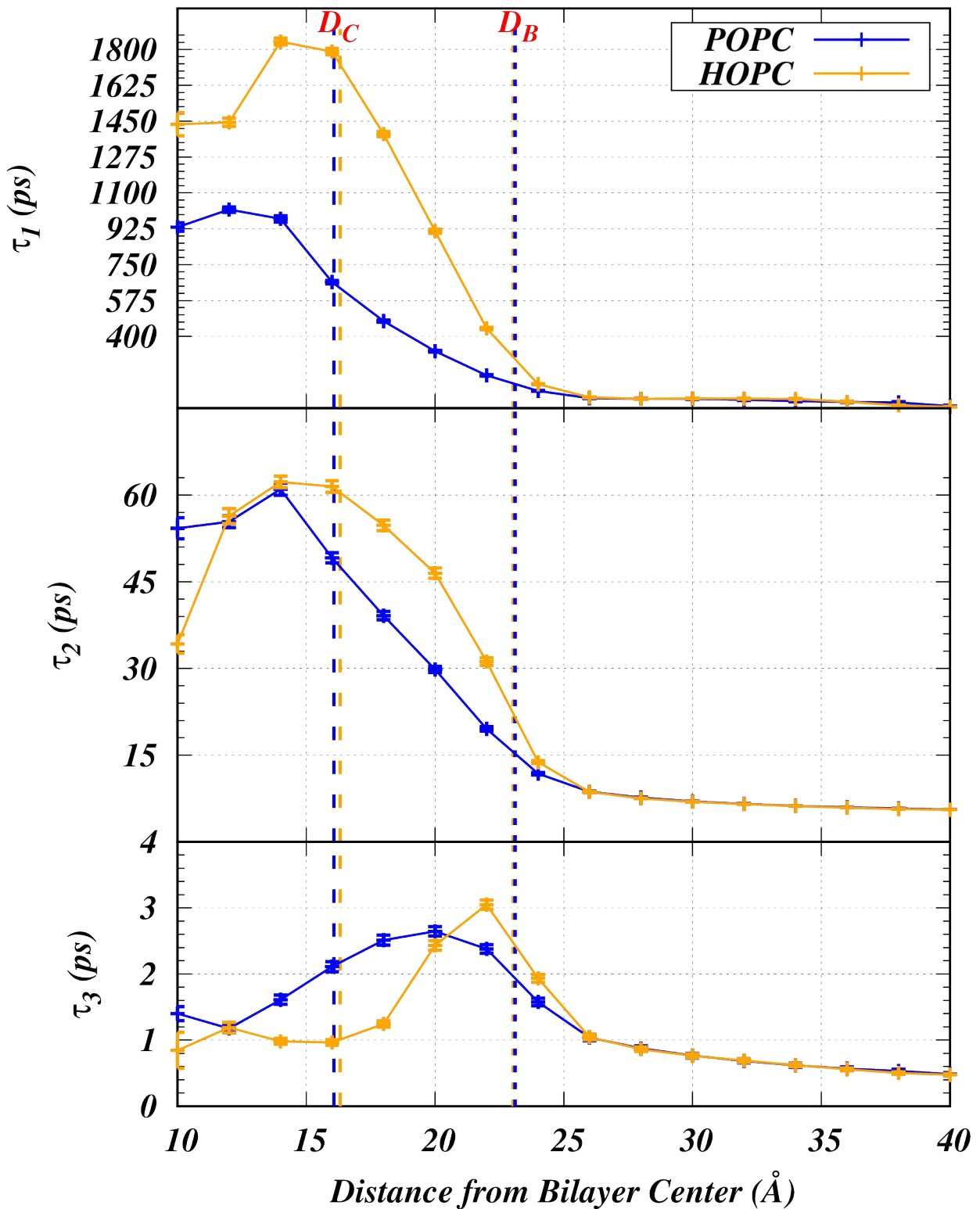


Figure 2.8: Orientational autocorrelation times of O-H bonds in water, as determined by modeling their autocorrelations using three-exponential fits. No values are shown for distances less than 12 Å from the bilayer center, as there are no waters in this region. The dashed vertical lines indicate chain boundaries  $D_c$  and bilayer thickness  $D_b/2$ , colored to indicate the lipid system.

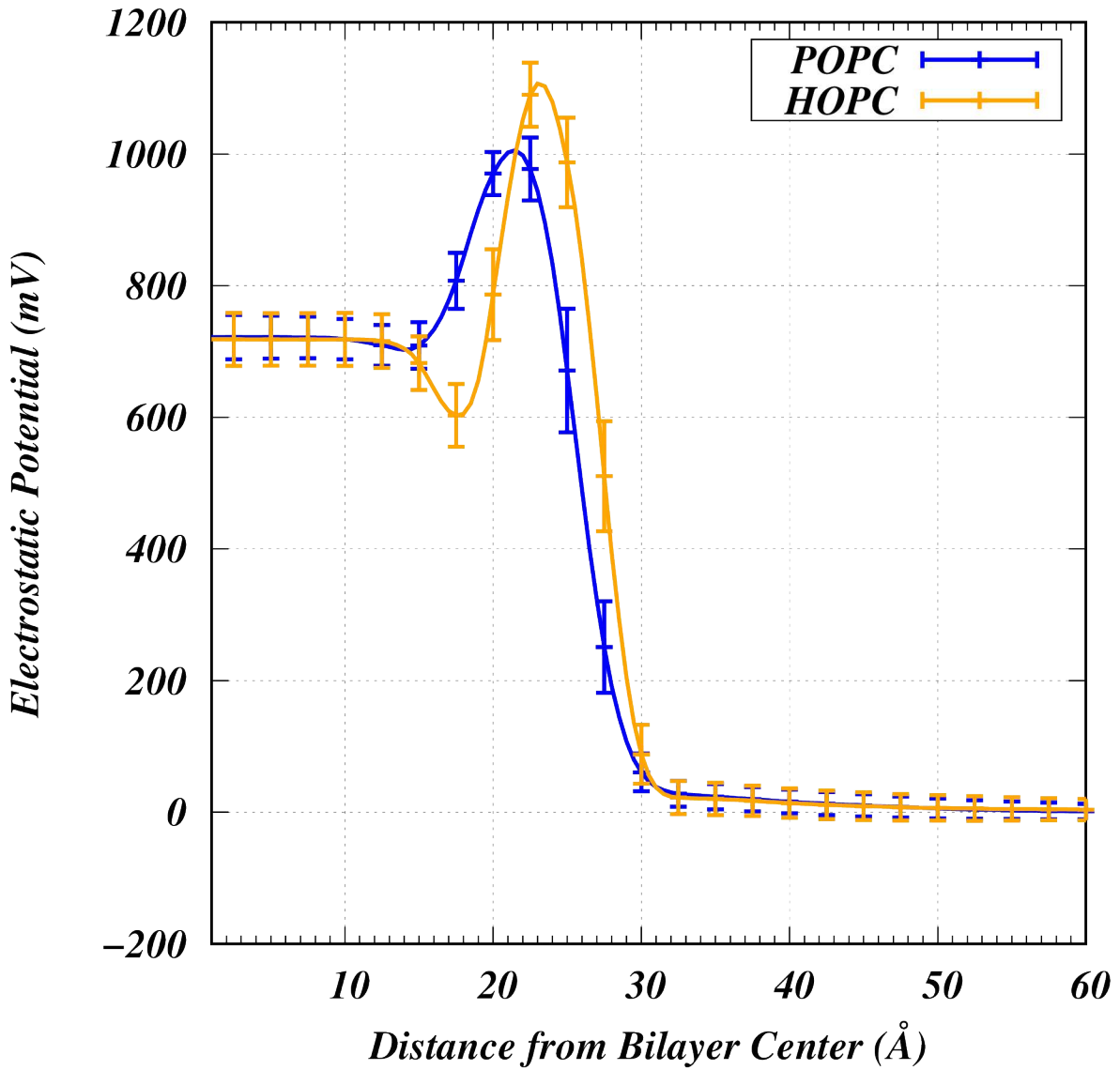


Figure 2.9: Comparison of electrostatic potentials between the HOPC and POPC systems. These distributions are calculated by integrating the charge density of our systems twice, assuming the the potential goes to zero at the box edge and that the electric field of bulk solvent is zero. Looking to the region from the bilayer center to around 10 Å, one can see the bilayer dipole potential. We see very similar values for this in both systems. We also see a large peak in the HOPC system, and a large trough that is not present in POPC. The larger peak at the bilayer surface may provide a barrier to solvent and dissolved ions, and the trough may be a trap that causes the buildup of solvent in the bilayer headgroup region.

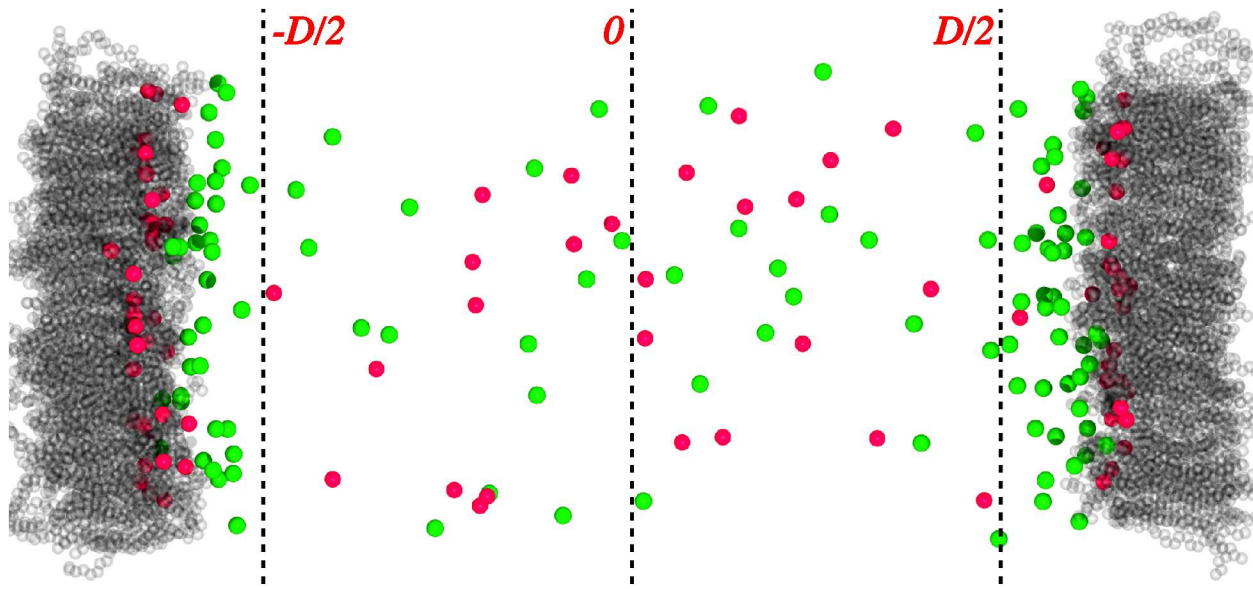


Figure 2.10: Illustration of bulk ion distribution, with surfaces used in Gouy-Chapman theory calculations. For the purpose of illustration, solvent has been hidden from this image. Cl<sup>-</sup> ions have been colored in green, and Na<sup>+</sup> ions are shown in red. Surfaces set at the *hydration boundary* of each bilayer leaflet are shown with dotted lines. The center of the solvent occupied region of the box is set at zero.

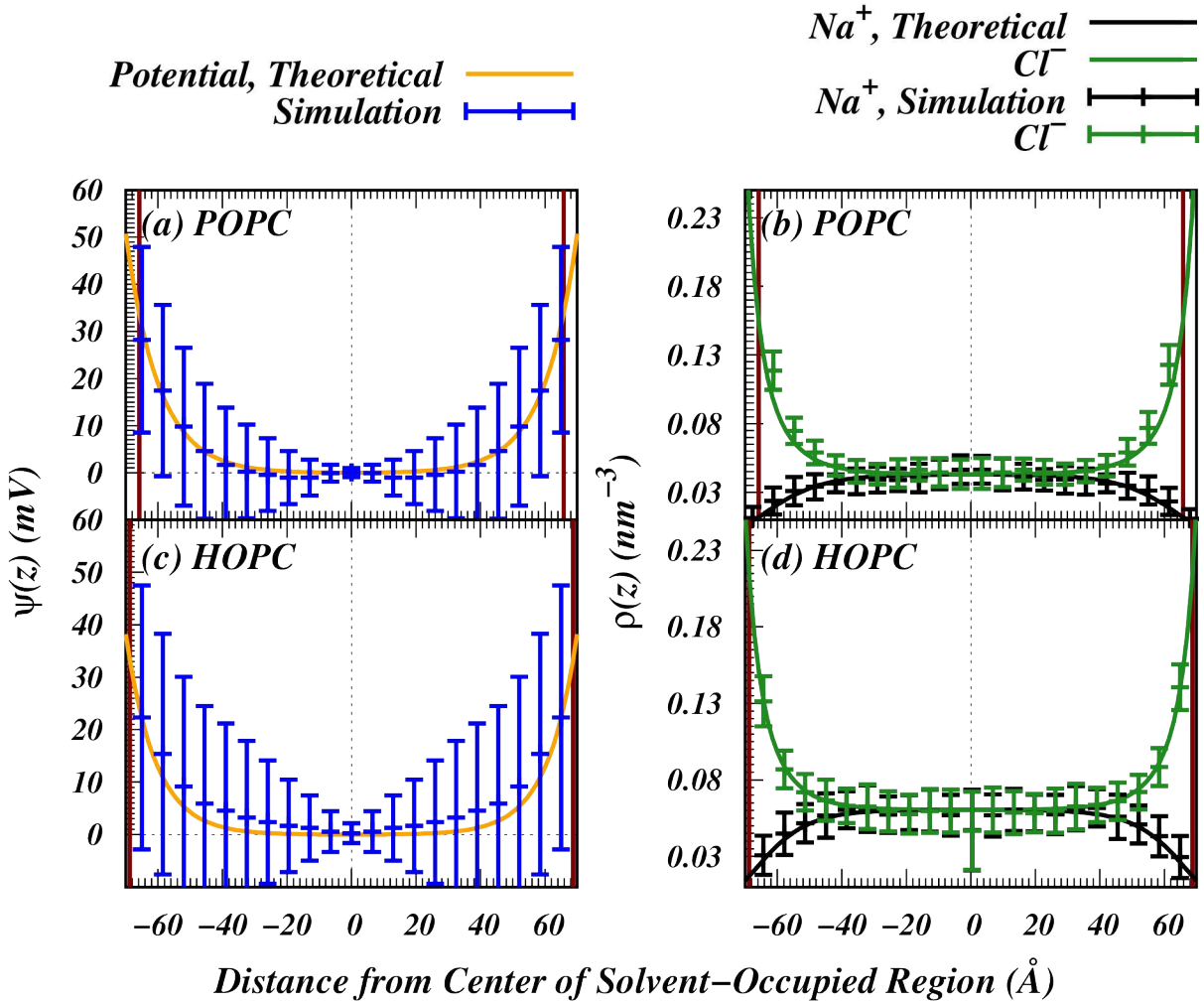


Figure 2.11: Comparison of Gouy-Chapman theory predictions and simulation results. Theoretical distributions are given by the solid lines, and data from our simulations are shown as points with error bars. (a) and (c) show the electrostatic potentials of each system. For clarity, we show error-bars for the simulation results for every 13th point. The Debye-Huckle potentials shown follow the form given in equation 2.12. (b) and (d) show the number density distribution of ions in each system. Error-bars for the simulation results are shown for every 30th point. Note that both systems are translated to center around the solvent-occupied region of the box, giving an interspace region of  $\sim 13$  nm in each system. Parameters used in Gouy-Chapman theory are in table 2.3

# Chapter 3

## Conclusions

Ether-linked lipid bilayers show a distinct peak in solvent density that is not disrupted by the inclusion of a moderate concentration of salt. This region shows significantly reduced lateral diffusion, and longer autocorrelation times than the same region in an analogous ester-linked lipid bilayer. Furthermore, we find that the characteristic lower dipole potential of an ether-linked bilayer reported in previous work [9] is increased to match that of the ester-linked bilayer in the presence of salt. We also find that, with our new protocol for determining the interface boundary of the lipid bilayer, our simulations model ion distributions and electrostatic potentials from Gouy-Chapman theory well. The shorter screening length in the ether-linked system suggests better shielding from electric fields far from the bilayer compared to the ester-linked system. This is a result of the ether-linked lipid bilayer's lower affinity for ions than the ester-linked analog.

# Bibliography

- [1] S. A. Pandit, H. L. Scott, Simulations and models of lipid bilayers, *Soft Matter: Lipid Bilayers and Red Blood Cells* 4 (2008) 1–82.
- [2] S. Sehgal, M. Kates, N. Gibbons, Lipids of halobacterium cutirubrum, *Canadian journal of biochemistry and physiology* 40 (1) (1962) 69–81.
- [3] Y. Koga, From promiscuity to the lipid divide: on the evolution of distinct membranes in archaea and bacteria, *Journal of molecular evolution* 78 (3-4) (2014) 234–242.
- [4] S. D. Guler, D. D. Ghosh, J. Pan, J. C. Mathai, M. L. Zeidel, J. F. Nagle, S. Tristram-Nagle, Effects of ether vs. ester linkage on lipid bilayer structure and water permeability, *Chemistry and physics of lipids* 160 (1) (2009) 33–44.
- [5] M. Jansen, A. Blume, A comparative study of diffusive and osmotic water permeation across bilayers composed of phospholipids with different head groups and fatty acyl chains, *Biophysical journal* 68 (3) (1995) 997–1008.
- [6] K. Gawrisch, D. Ruston, J. Zimmerberg, V. Parsegian, R. Rand, N. Fuller, Membrane dipole potentials, hydration forces, and the ordering of water at membrane surfaces, *Biophysical journal* 61 (5) (1992) 1213–1223.
- [7] N. S. Haas, P. Sripada, G. G. Shipley, Effect of chain-linkage on the structure of phosphatidyl choline bilayers. hydration studies of 1-hexadecyl 2-palmitoyl-sn-glycero-3-phosphocholine, *Biophysical journal* 57 (1) (1990) 117–124.

- [8] J. C. Fogarty, M. Arjunwadkar, S. A. Pandit, J. Pan, Atomically detailed lipid bilayer models for the interpretation of small angle neutron and x-ray scattering data, *Biochimica et Biophysica Acta (BBA)-Biomembranes* 1848 (2) (2015) 662–672.
- [9] J. Kruczak, M. Saunders, M. Khosla, Y. Tu, S. A. Pandit, Molecular dynamics simulations of ether-and ester-linked phospholipids, *Biochimica et Biophysica Acta (BBA)-Biomembranes* 1859 (12) (2017) 2297–2307.
- [10] A. N. Leonard, R. W. Pastor, J. B. Klauda, Parameterization of the charmm all-atom force field for ether lipids and model linear ethers, *The Journal of Physical Chemistry B* (2018).
- [11] J. Kruczak, S.-W. Chiu, E. Jakobsson, S. A. Pandit, Effects of lithium and other monovalent ions on palmitoyl oleoyl phosphatidylcholine bilayer, *Langmuir* 33 (4) (2017) 1105–1115, pMID: 28076953, arXiv:<http://dx.doi.org/10.1021/acs.langmuir.6b04166>, doi:[10.1021/acs.langmuir.6b04166](https://doi.org/10.1021/acs.langmuir.6b04166). URL <http://dx.doi.org/10.1021/acs.langmuir.6b04166>
- [12] N. Duro, M. Gjika, A. Siddiqui, H. L. Scott, S. Varma, Popc bilayers supported on nanoporous substrates: specific effects of silica-type surface hydroxylation and charge density, *Langmuir* 32 (26) (2016) 6766–6774.
- [13] G. Pabst, A. Hodzic, J. Štrancar, S. Danner, M. Rappolt, P. Laggner, Rigidification of neutral lipid bilayers in the presence of salts, *Biophysical journal* 93 (8) (2007) 2688–2696.
- [14] J. N. Sachs, H. Nanda, H. I. Petracche, T. B. Woolf, Changes in phosphatidylcholine headgroup tilt and water order induced by monovalent salts: molecular dynamics simulations, *Biophysical journal* 86 (6) (2004) 3772–3782.

- [15] H. I. Petrache, S. Tristram-Nagle, D. Harries, N. Kučerka, J. F. Nagle, V. A. Parsegian, Swelling of phospholipids by monovalent salt, *Journal of lipid research* 47 (2) (2006) 302–309.
- [16] J.-P. Douliez, A. Leonard, E. J. Dufourc, Restatement of order parameters in biomembranes: calculation of cc bond order parameters from cd quadrupolar splittings., *Biochemical journal* 68 (5) (1995) 1727.
- [17] M. J. Abraham, T. Murtola, R. Schulz, S. Páll, J. C. Smith, B. Hess, E. Lindahl, Gromacs: High performance molecular simulations through multi-level parallelism from laptops to supercomputers, *SoftwareX* 1 (2015) 19–25.
- [18] S. Pall, M. J. Abraham, C. Kutzner, B. Hess, E. Lindahl, Tackling exascale software challenges in molecular dynamics simulations with gromacs, in: International Conference on Exascale Applications and Software, Springer, 2014, pp. 3–27.
- [19] D. V. D. Spoel, E. Lindahl, B. Hess, G. Groenhof, A. Mark, H. Berendsen, Gromacs: fast, flexible, free, *J. Comput. Chem.* 26 (2005) 1701.
- [20] E. Lindahl, B. Hess, D. Van Der Spoel, Gromacs 3.0: a package for molecular simulation and trajectory analysis, *Molecular modeling annual* 7 (8) (2001) 306–317.
- [21] H. J. Berendsen, D. van der Spoel, R. van Drunen, Gromacs: a message-passing parallel molecular dynamics implementation, *Computer Physics Communications* 91 (1-3) (1995) 43–56.
- [22] H. Berendsen, J. Grigera, T. Straatsma, The missing term in effective pair potentials, *Journal of Physical Chemistry* 91 (24) (1987) 6269–6271.
- [23] S.-W. Chiu, S. A. Pandit, H. Scott, E. Jakobsson, An improved united atom force field for simulation of mixed lipid bilayers, *The Journal of Physical Chemistry B* 113 (9) (2009) 2748–2763.

- [24] I. S. Joung, T. E. Cheatham III, Determination of alkali and halide monovalent ion parameters for use in explicitly solvated biomolecular simulations, *The journal of physical chemistry B* 112 (30) (2008) 9020–9041.
- [25] S. Nosé, M. Klein, Constant pressure molecular dynamics for molecular systems, *Molecular Physics* 50 (5) (1983) 1055–1076.
- [26] M. Parrinello, A. Rahman, Polymorphic transitions in single crystals: A new molecular dynamics method, *Journal of Applied physics* 52 (12) (1981) 7182–7190.
- [27] B. Hess, H. Bekker, H. J. C. Berendsen, J. G. E. M. Fraaije, Lincs: A linear constraint solver for molecular simulations, *Journal of Computational Chemistry* 18 (12) (1997) 1463–1472.  
doi:10.1002/(SICI)1096-987X(199709)18:12<1463::AID-JCC4>3.0.CO;2-H.  
URL [http://dx.doi.org/10.1002/\(SICI\)1096-987X\(199709\)18:12<1463::AID-JCC4>3.0.CO;2-H](http://dx.doi.org/10.1002/(SICI)1096-987X(199709)18:12<1463::AID-JCC4>3.0.CO;2-H)
- [28] U. Essmann, L. Perera, M. L. Berkowitz, T. Darden, H. Lee, L. G. Pedersen, A smooth particle mesh ewald method, *The Journal of chemical physics* 103 (19) (1995) 8577–8593.
- [29] H. I. Petracche, S. E. Feller, J. F. Nagle, Determination of component volumes of lipid bilayers from simulation, *Biophysical Journal* 72 (5) (1997) 2237–2242.  
URL <http://www.ncbi.nlm.nih.gov/pmc/articles/PMC1184418/>
- [30] E. Egberts, H. Berendsen, Molecular dynamics simulation of a smectic liquid crystal with atomic detail, *The Journal of chemical physics* 89 (6) (1988) 3718–3732.
- [31] S. Varma, S. B. Rempe, Structural transitions in ion coordination driven by changes in competition for ligand binding, *Journal of the American Chemical Society* 130 (46) (2008) 15405–15419.

- [32] K. Åman, E. Lindahl, O. Edholm, P. Håkansson, P.-O. Westlund, Structure and dynamics of interfacial water in an  $l\alpha$  phase lipid bilayer from molecular dynamics simulations, *Biophysical journal* 84 (1) (2003) 102–115.
- [33] P. Dutta, M. Botlani, S. Varma, Water dynamics at protein–protein interfaces: Molecular dynamics study of virus–host receptor complexes, *The Journal of Physical Chemistry B* 118 (51) (2014) 14795–14807.
- [34] M. L. Berkowitz, D. L. Bostick, S. Pandit, Aqueous solutions next to phospholipid membrane surfaces: insights from simulations, *Chemical reviews* 106 (4) (2006) 1527–1539.
- [35] A. Cordomi, O. Edholm, J. J. Perez, Effect of ions on a dipalmitoyl phosphatidylcholine bilayer. a molecular dynamics simulation study, *The Journal of Physical Chemistry B* 112 (5) (2008) 1397–1408.
- [36] J. N. Israelachvili, *Intermolecular and surface forces*, Academic press, 2011.
- [37] P. Wiersema, A. Loeb, J. T. G. Overbeek, Calculation of the electrophoretic mobility of a spherical colloid particle, *Journal of Colloid and Interface Science* 22 (1) (1966) 78–99.

### 3.1 Supplemental Figures and Captions

Table S1: Component volumes calculated from number densities using the method outlined by Petrache *et al.* [29]. Values for each headgroup component are difficult to determine uniquely due to significant overlap in their number density distribution, as well as the volume per each  $CH_1$  group.

Figure S1: X-ray scattering formfactors from simulated systems. These are the cosine transform of the electron densities for POPC (a) and HOPC (b).

	Water & Ions	P&N	HG Oxy-gens	HG Carbons	CH <sub>2</sub>	CH <sub>1</sub>	CH <sub>3</sub>
HOPC	29.96 ± 0.003989	24.43 ± 0.5058	2.589 ± 0.4493	22.59 ± 0.3381	26.57 ± 0.06971	23.9 ± 0.4969	53.98 ± 0.2396
POPC	29.99 ± 0.002374	20.61 ± 1.045	8.651 ± 0.2112	20.84 ± 0.3946	26.5 ± 0.1096	24.28 ± 0.685	53.72 ± 0.408

Table S1

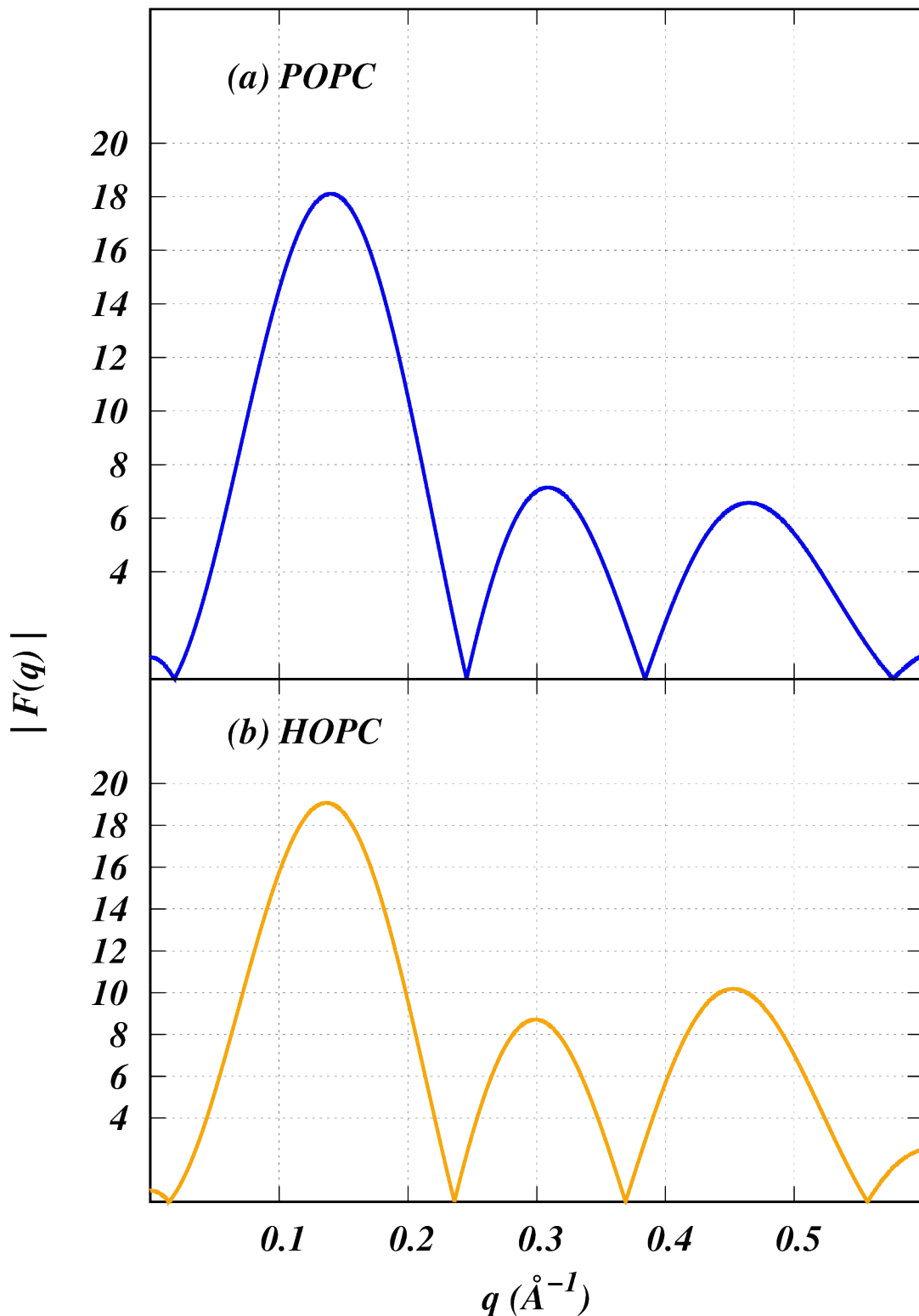


Figure S1